Journal of Alloys and Compounds 509 (2011) 7789–7793

Contents lists available at ScienceDirect

Journal of Alloys and Compounds

journal homepage: www.elsevier.com/locate/jallcom

Photoluminescence and energy transfer of Ce^{3+} and Tb^{3+} doped oxyfluoride aluminosilicate glasses

Ligang Zhu [a,b,*], Anxian Lu [a], Chenggang Zuo [a], Weiqun Shen [b]

[a] School of Materials Science and Engineering, Central South University, Changsha 410083, China
[b] School of Chemistry and Materials Science, Yulin Normal University, Yulin 537000, China

ARTICLE INFO

Article history:
Received 8 December 2010
Received in revised form 25 April 2011
Accepted 27 April 2011
Available online 10 May 2011

Keywords:
Ce^{3+}, Tb^{3+} rare earth ions
Oxyfluoride glass
Luminescence
Energy transfer

ABSTRACT

The transmission and photoluminescence (PL) properties of Ce^{3+} or Tb^{3+} doped and Tb^{3+}/Ce^{3+} codoped oxyfluoride aluminosilicate glasses were reported. The X-ray diffraction (XRD) and differential scanning calorimetry (DSC) were applied to confirm the structure and thermal stability of samples. PL spectra revealed a bright and broad violet-blue emission derived from Ce^{3+} [5d (^{2}D) → $^2F_{5/2,7/2}$] and an intense sharp green emission (543 nm) derived from Tb^{3+} ($^5D_4 \rightarrow {}^7F_5$) in the Ce^{3+} and Tb^{3+} doped glasses, respectively. Concentration quenching is not observed even the mole ratio of Tb^{3+} is up to 8% in Tb^{3+} doped glass. This indicates that the as-made host glass provides a good distribution of Tb^{3+} activators in glass matrix. For Tb^{3+}/Ce^{3+} codoped glasses, a strong green emission corresponding to Tb^{3+} ($^5D_4 \rightarrow {}^7F_5$) and an energy transfer phenomenon from Ce^{3+} to Tb^{3+} were observed upon excitation with an UV wavelength (289 nm). It was also observed that their PL intensity depends on the concentration of Ce^{3+} when the concentration of Tb^{3+} is fixed. The mechanism involved in the energy transfer between Ce^{3+} and Tb^{3+} was explained with an energy level diagram.

1. Introduction

Rare earth (RE) ions possess unique optical behavior and play an important role in the development of many optoelectronic devices such as lasers, colour displays, light converters, optical fibers and amplifiers [1–3]. Over the past few years, there has been a considerable interest in the study of RE doped glasses due to their high efficiency luminescence, as well as their transparent, easy-shaping and cost-effective properties [4]. One of the important criteria for obtaining high efficiency luminescence from RE elements in glasses is that the glass matrix possesses low phonon energies. Transparent oxyfluoride glasses doped with RE ions were studied extensively in the past decades, since such materials provide a desirable low phonon energy environment for activator ions similar to fluoride glasses, and keep high mechanical strength, chemical durability, and thermal stability typical for oxide glasses [5].

In the present work, we have undertaken the oxyfluoride aluminosilicate glasses to study the spectral properties of Ce^{3+} and Tb^{3+} ions. Terbium is widely used as activators in different host materials to obtain green light [6,7]. The Tb^{3+} fluorescence under UV excitation in most host matrixes consists of four main emission bands around 490 (blue), 545 (green), 580 (yellow) and 620 (red) nm, which correspond to the $^5D_4 \rightarrow {}^7F_J$ (J = 6–3) transitions [8]. Furthermore, the emission ($^5D_4 \rightarrow {}^7F_5$, about 545 nm) mostly dominates over all other emissions, so the Tb^{3+} fluorescence usually appears green to the human eye.

Although oxyfluoride aluminosilicate glass is an excellent luminescence matrix, there are many point defects in the glass where electrons and holes can be entrapped, resulting in non-radiative recombination processes [9]. In order to improve the emission performance of Tb^{3+}, some suitable sensitizers were usually added to the glass matrix [10]. It is well known that Ce^{3+} is also a high efficiency emission center because the 4f–5d transitions of Ce^{3+} are allowed by the Laporte parity selection rules [11]. Moreover, Ce^{3+} has been proved to be an efficient sensitizer, especially for Tb^{3+}, and the energy transfer processes between Ce^{3+} and Tb^{3+} in different hosts have been extensively investigated, such as borate glass [12], borosilicate glass [13] and phosphate glass [14]. However, little attention has been paid to the luminescence properties of Tb^{3+}/Ce^{3+} codoped oxyfluoride glasses [15,16]. In this work, Tb^{3+} or Ce^{3+} doped and Tb^{3+}/Ce^{3+} codoped oxyfluoride aluminosilicate glasses were successfully prepared. XRD, optical transmission, and luminescence behavior under UV were investigated. Energy transfer from Ce^{3+} to Tb^{3+}, which improved the

* Corresponding author at: School of Materials Science and Engineering, Central South University, Changsha 410083, China. Tel.: +86 73188830351; fax: +86 73188877057.
E-mail address: zhuligang1@163.com (L. Zhu).

0925-8388/$ – see front matter © 2011 Elsevier B.V. All rights reserved.
doi:10.1016/j.jallcom.2011.04.154

green emission performance of Tb^{3+} in the codoped glasses was discussed.

2. Experimental details

2.1. Glasses preparation

Following are the Tb^{3+} or Ce^{3+} ions doped and Tb^{3+}/Ce^{3+} codoped oxyfluoride aluminosilicate glasses that are developed for the present work along with a reference glass.

$50SiO_2–15Al_2O_3–20LiF–15CaF_2–0.2Sb_2O_3$(hostglass)(mol.%)

$50SiO_2–15Al_2O_3–20LiF–15CaF_2–0.2Sb_2O_3–1.0Ce_2O_3$

$50SiO_2–15Al_2O_3–20LiF–15CaF_2–0.2Sb_2O_3–xTb_2O_3$

$\times x =$ 0.25, 0.5, 1.0, 2.0, 4.0, 6.0, 8.0)

$50SiO_2–15Al_2O_3–20LiF–15CaF_2–0.2Sb_2O_3–1.0Tb_2O_3–xCe_2O_3$

$\times (x =$ 0.25, 0.5, 1.0, 1.5, 2.0)

All these glasses were prepared from analytical reagent SiO_2, Al_2O_3, LiF, CaF_2, Sb_2O_3 and 4N-purity grade Ce_2O_3, Tb_4O_7 raw materials. Here, Sb_2O_3 was used as reducing agents. Thus, a reducing atmosphere was created and the formation of Ce^{4+} ions was depressed. For convenience, we labelled $50SiO_2–15Al_2O_3–20LiF–15CaF_2–0.2Sb_2O_3–1.0Ce_2O_3$ glass as C1, $50SiO_2–15Al_2O_3–20LiF–15CaF_2–0.2Sb_2O_3–xTb_2O_3$ (x = 0.25, 0.5, 1.0, 2.0, 4.0, 6.0, 8.0) glasses as T1, T2, T3, T4, T5, T6 and T7, respectively, and $50SiO_2–15Al_2O_3–20LiF–15CaF_2–0.2Sb_2O_3–1.0Tb_2O_3–xCe_2O_3$ (x = 0.25, 0.5, 1.0, 1.5, 2.0) glasses as TC1, TC2, TC3, TC4 and TC5, respectively. Each batch weighing about 50 g was mixed homogeneously and melted at 1500 °C for 2 h in a covered corundum crucible in air. The melts were poured into a pre-heated stainless steel mold. The resultant glasses were annealed in a muffle furnace at 500 °C for 2 h to release the inner stress. All the glasses were homogeneous and transparent with a regular size of 3 cm × 2 cm × 0.2 cm after cutting and polishing.

2.2. Measurements

The densities of the glasses were measured using the buoyancy method based on the Archimedes principle with toluene as an immersion liquid. The powder XRD profiles were obtained on a Rigaku D/Max 2500 powder diffractometer with Cu K_α radiation (λ = 1.5406 Å). DSC data were obtained with a Netzsch STA 449 C in the temperature range of 30–1200 °C, at the rate of 10 °C/min, under N_2 atmosphere. The ultraviolet–visible (UV–vis) transmission spectra were measured by Shimadzu UV-2550 spectrophotometer. The PL curves were recorded on a Hitachi F-2500 fluorescence spectrophotometer (resolution 0.3 nm) equipped with a Xe lamp as the excitation source at room temperature. The excitation and emission slits were set at 2.5 nm, all the spectra were measured at a scan speed of 300 nm/min under a PMT voltage of 400 V. On the basis of the signal to noise ratios, the relative errors in the spectral measurements are estimated to be ±2%.

3. Results and discussion

Fig. 1 presents the representative XRD profile of as-made glasses, which confirms its amorphous structural nature since no diffraction peaks was found. In addition, the XRD profiles of Tb^{3+} or Ce^{3+} doped and other Tb^{3+}/Ce^{3+} codoped glasses were similar to that of Fig. 1. Table 1 presents the physical properties of Tb^{3+} (T3 as the representative) or Ce^{3+} doped and Tb^{3+}/Ce^{3+} (TC3 as the representative) codoped glasses. The representative DSC thermograms of Tb^{3+} or Ce^{3+} doped and Tb^{3+}/Ce^{3+} codoped glasses are shown in Fig. 2. From these profiles, the glass transition temperature (T_g), crystallization temperature (T_{c1} and T_{c2}) and melting temperature (T_m) of T3, C1, and TC3 glasses have been identified, and the glass stability factor (S) and Hruby's parameter (K_{gl}) have been obtained from these values and listed in Table 1. The thermal stability factor (ΔT) has frequently been used to understand the glass stability. The obtained glass stability factors reveal that these glasses are more stable. Hruby's parameter gives information on the stability of the glass against devitrification.

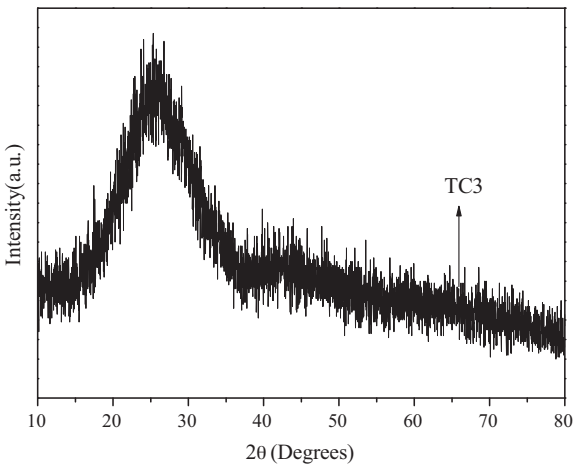

Fig. 1. XRD profile of the representative glass.

Table 1
Physical properties of 1.0 mol.% Tb^{3+} or Ce^{3+} doped and Tb^{3+}/Ce^{3+} codoped oxyfluoride aluminosilicate glasses.

Physical quantities	Results		
	T3	C1	TC3
Average molecular weight, M (g)	65.69	65.31	68.25
Density, d (g/cm^3)	2.653	2.645	2.754
Thickness, t (cm)	0.2	0.2	0.2
Number density, N ($\times 10^{22}$ ions/cm^3)	2.431	2.438	2.429
Molar volume, V_m (cm^3)	24.761	24.692	24.782
Glass transition temperature, T_g (°C)	564	565	576
Crystallization temperature, T_{c1} (°C)	717	720	730
T_{c2} (°C)	798	783	796
Temperature of melting, T_m (°C)	972	965	964
Glass stability factor, $S = T_{c1} - T_g$ (°C)	153	155	154
Hruby's parameter, $K_{gl} = (T_{c1} - T_g)/(T_m - T_{c1})$	0.600	0.633	0.658

The UV–vis transmission spectra of Tb^{3+} (T3 as the representative) or Ce^{3+} doped and Tb^{3+}/Ce^{3+} codoped glasses (TC3 as the representative) are shown in Fig. 3. For Ce^{3+} doped glass, Ce^{3+} ion exhibits a broad absorption band in the UV with an absorption edge about 351 nm (T = 50%), which is caused by the 4f–5d transition of Ce^{3+} ion. Several weak absorption peaks centered at 350, 367, 377 and 484 nm arising from f–f transitions in the visible region and an UV absorption edge at about 310 nm (T = 50%) are observed in the Tb^{3+} doped glass. With regard to the Tb^{3+}/Ce^{3+} codoped glass,

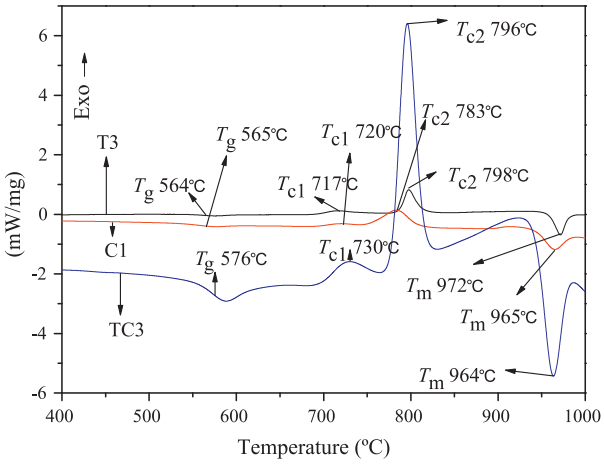

Fig. 2. DSC profiles of the (1.0 mol.%) Tb^{3+} or Ce^{3+} doped and Tb^{3+}/Ce^{3+} codoped glasses.

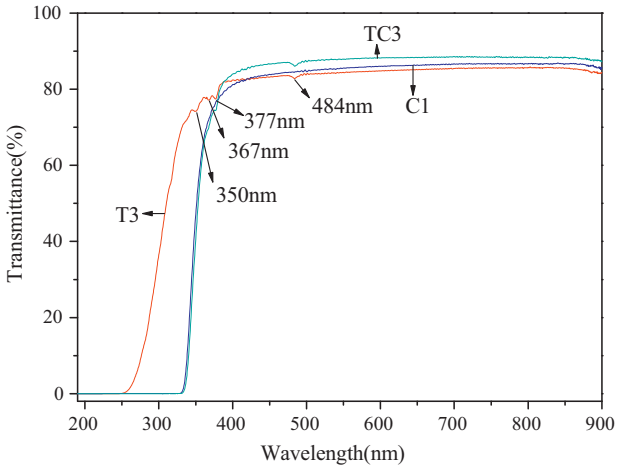

Fig. 3. UV–vis transmission spectra of the (1.0 mol.%) Tb^{3+} or Ce^{3+} doped and Tb^{3+}/Ce^{3+} codoped glasses.

absorption peaks at the shorter wavelengths corresponding to f–f transitions of Tb^{3+} ion are overlapped because of 4f–5d transition of Ce^{3+} ion. In comparison with Tb^{3+} doped glass, the UV absorption edge shifts to longer wavelength at about 353 nm (T = 50%) from Tb^{3+}/Ce^{3+} codoped glass. The redshift of the UV absorption edge is mainly because of two factors: the interconfigurational transition of Ce^{3+}, and the increase of non-bridge oxygen which results from the increase of the O/Si mole ratio with the addition of Ce^{3+} [16].

It is well known that the absorption of Ce^{4+} ion is a charge transfer from O^{2-} to Ce^{4+} and the position of the band is usually located at longer wavelength in comparison with that of Ce^{3+} ion. Ce^{4+} ion in oxide glasses made under an air atmosphere had an absorption edge at about 450 nm [17]. In this study, the absorption edge shifted to 351, 353 nm by employing a reducing atmosphere with Sb_2O_3, indicating that cerium mainly exists as Ce^{3+} in those glass samples.

Fig. 4a presents the excitation spectrum of the 1.0 mol.% Ce^{3+} ions doped glass, monitored with an emission wavelength of 385 nm. The excitation spectrum shows a strong excitation band centered at 334 nm along with a comparative weak band at 292 nm, which is assigned to the $4f^1 \rightarrow 5d^1$ transitions of Ce^{3+} ions. The emission spectrum of the 1.0 mol. % Ce^{3+} ions doped glass is shown in Fig. 4b with 334 nm excitation wavelength. In the case of Ce^{3+}, when excited by VUV/UV light, the lone electron goes to one of the excited 5d levels. Generally, upon de-excitation to the ground level, two prominent bands are observed separated by few thousand cm^{-1} due to the transitions from the lowest 5d level to the spin-orbit split $^2F_{5/2}$ and $^2F_{7/2}$ states of the $4f^1$ configuration [18]. In this work, these two transitions are merged with each other due to the strong inhomogeneous broadening and as a result a strong broad asymmetric band is observed. According to the asymmetric curve shape and position, the spectrum was de-convoluted (Gaussian fit) into two peaks (382 and 405 nm), which is shown in the inset of Fig. 4b. The energy difference between 382 and 405 nm is 1487 cm^{-1}, basically agreeing with the ground state splitting of Ce^{3+} ions as discussed above.

The excitation and emission spectra for Tb^{3+} ions doped glasses with different Tb-doping contents were illustrated in Fig. 5a and b, respectively. The excitation spectra were obtained by monitoring the green emission at 543 nm. The overall excitation spectra consist of the $4f^8 \rightarrow 4f^7 5d^1$ transitions of Tb^{3+} in the short UV region (230–300 nm) and $4f^8 \rightarrow 4f^8$ transitions in the longer wavelength region (300–500 nm). The Tb^{3+} has a $4f^8$ electron configuration and prefers to give away one electron forming a more stable half-filled $4f^7$ configuration, so that the strong band at 241 nm and the relatively weak band at 283 nm have been observed easily to be the spin-allowed and spin-forbidden f–d transitions, respectively. The energy difference between the bands at 241 and 283 nm is about 6150 cm^{-1}, which approximately equals to the average energy difference between the spin-allowed and spin-forbidden f–d transitions for Tb^{3+} (6000 cm^{-1}) [19]. In the longer wavelength region, the f–f transition lines of Tb^{3+} are assigned as the transitions from the $^7F_6$ ground state to the different excited states, i.e., 303 nm ($^5H_6$), 317 nm ($^5H_7$, $^5D_0$), 340 nm ($^5L_7$), 351 nm ($^5L_8$, $^5G_3$, $^5L_9$, $^5G_4$, $^5D_2$, $^5G_5$), 369 nm ($^5L_{10}$), 378 nm ($^5D_3$) and 485 nm ($^5D_4$), respectively [20].

Only the prominent excitation peak at 378 nm ($^7F_6 \rightarrow {}^5D_3$) has been selected for the measurement of emission spectra. The emission transitions have shown sharp emission bands due to the f–f inner shell transitions, from the excited level to the lower level such as $^5D_4 \rightarrow {}^7F_J$ (J = 3–6) for Tb^{3+}. When Tb^{3+} ions are excited by UV radiation, electronic transition of either $^5D_3 \rightarrow {}^7F_J$ (blue emission) or successive $^5D_3 \rightarrow {}^5D_4$ and $^5D_4 \rightarrow {}^7F_J$ (green emission) takes place, where J = 3–6. Bands with smaller widths and larger intensities are noticed from 480 to 630 nm. From emission spectra, transitions such as $^5D_4 \rightarrow {}^7F_6$ (489 nm), $^5D_4 \rightarrow {}^7F_5$ (543 nm), $^5D_4 \rightarrow {}^7F_4$ (585 nm) and $^5D_4 \rightarrow {}^7F_3$ (622 nm) have been identified [20–22]. Of them, 543 nm has shown bright green emission, arising from the Laporte-forbidden $^5D_4 \rightarrow {}^7F_5$ transition. The transition $^5D_4 \rightarrow {}^7F_6$ obeys the magnetic dipole (MD) transition selection rule of $\Delta J = \pm 1$ [22].

In the emission spectra, the line positions and widths do not change with the Tb^{3+} concentration, indicating the nature of Tb^{3+} activation is not influenced. On the other hand, the PL intensities altered with Tb^{3+} concentration, as shown in Fig. 5b. It is very significant that Tb^{3+} can be doped up to 8.0 mol.% in host glass without fluorescence quenching. The PL saturation may result from a number of factors such as the non-radiative transition or cross-relaxation process brought about by Tb–Tb interactions. It is well known that the luminescent intensity is related to the average distance between luminescent centers. With the doping concentration increases, the distance between active ions decreases. When the distance is short enough, the interaction between active ions will occur and cause concentration quenching. Therefore, the homogeneous distribution of active ions in host glass is essential in order to acquire highly doped glasses without concentration quenching. As mentioned above, the as-made host glass provides a more homogeneous environment, and enhances the distribution of Tb^{3+}. The good distribution of Tb^{3+} activators could reduce the non-radiative relaxation, and result in an increase in the emission intensity and quenching concentration.

The Ce^{3+} ion is a well known sensitizer for certain trivalent RE metal ion luminescence, and the sensitizing effects depend strongly on the local environment into which these ions are introduced. The luminescence characteristics of Tb^{3+}/Ce^{3+} codoped glasses with different Ce-doping contents were explored. Its typical excitation and emission spectra are shown in Fig. 6. The excitation spectra (Fig. 6a) monitored with the 543 nm emission ($^5D_4 \rightarrow {}^7F_5$) of Tb^{3+} consist of the excitation bands of the Ce^{3+} and the Tb^{3+} ions, indicating that the Tb^{3+} ions are essentially excited through the Ce^{3+} ions. Thus, energy transfer from Ce^{3+} to Tb^{3+} ions exists in these samples. As the Ce-doping content increased from 0.25 to 2.0 mol.%, the intensity of $4f^1 \rightarrow 5d^1$ (289 nm) transition of Ce^{3+} ions increased at first and reached a maximum at 1.0 mol.%; subsequently, the intensity decreased.

To monitor the green emission (543 nm) of Tb^{3+}/Ce^{3+} codoped glasses with a fixed Tb^{3+} content (1 mol.%) and varied contents of the co-dopant Ce^{3+} (0.25, 0.5, 1.0, 1.5, 2.0 mol.%), an intense excitation band at 289 nm was used. The emission spectrum of the 1.0 mol.% Tb^{3+} ions doped glass with 378 nm excitation wavelength is also presented in the figure for comparison. From Fig. 6b, the

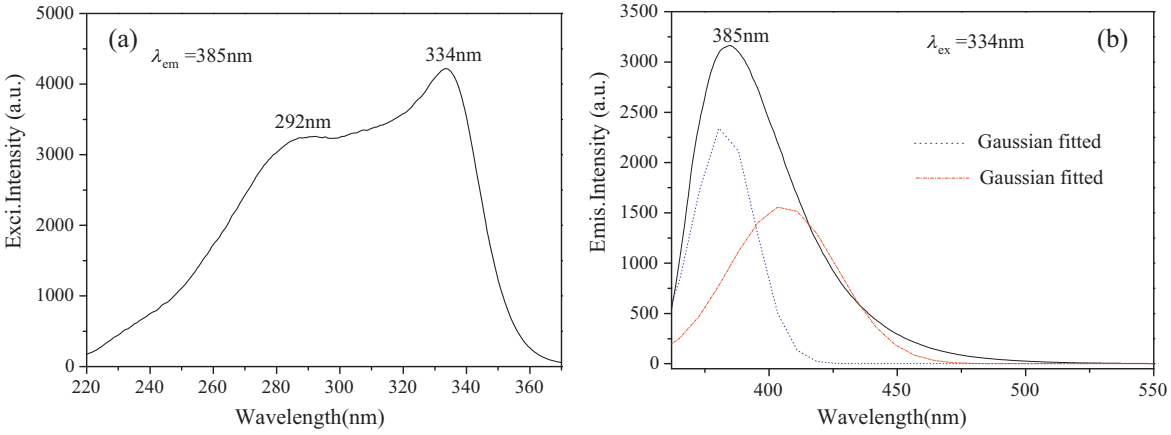

Fig. 4. Excitation (a) and emission (b) spectra of the (1.0 mol.%) Ce^{3+} ions doped glass.

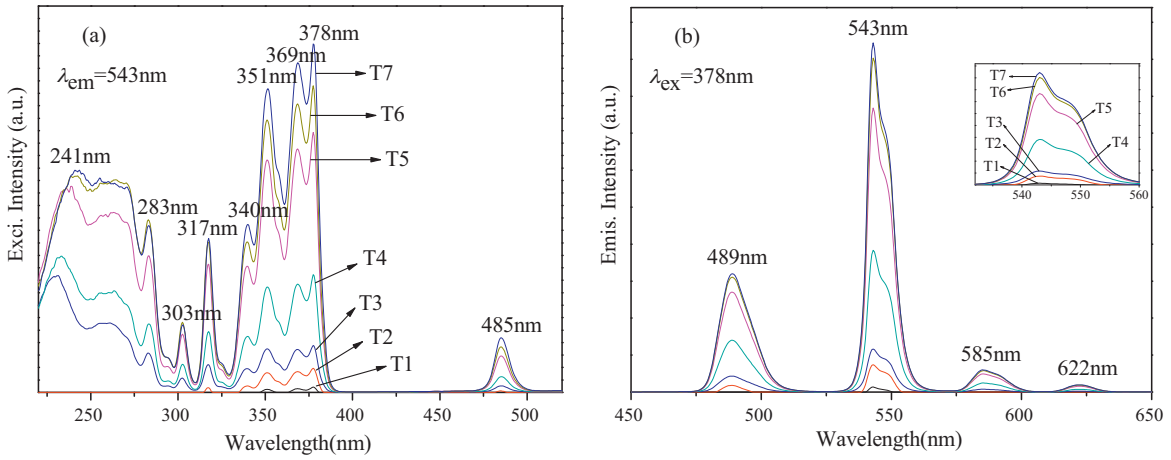

Fig. 5. Excitation (a) and emission (b) spectra of the Tb^{3+} ions doped glasses with different Tb-doping contents.

intense emissions of Tb^{3+} from the transitions $^5D_4 \rightarrow {}^7F_J$ (J = 6–3) have been observed. It indicates that an energy transfer from Ce^{3+} to Tb^{3+} occurs in these Tb^{3+}/Ce^{3+} codoped glasses. Fig. 6c shows the dependence of PL intensities ($^5D_4 \rightarrow {}^7F_5$ transition of Tb^{3+}) on Ce^{3+} concentration in the Tb^{3+}/Ce^{3+} codoped glasses. The enhancement of the green emission intensity of Tb^{3+} in the presence of Ce^{3+} upon excitation with an UV wavelength of 289 nm was observed. And the optimized concentration of cerium was identified as 1.0 mol.% based on its emission performance, as shown in Fig. 6c.

The energy transfer process from Ce^{3+} to Tb^{3+} is schematically depicted in Fig. 7. First, the UV photons (at 289 nm) are absorbed by Ce^{3+} ions, resulting in the Ce^{3+} ions excited to the $^5D_{5/2}$ level. Then, the excited Ce^{3+} ions in $^5D_{5/2}$ level may relax non-radiatively to the underlying excited level, $^5D_{3/2}$ level. Subsequently, the energy

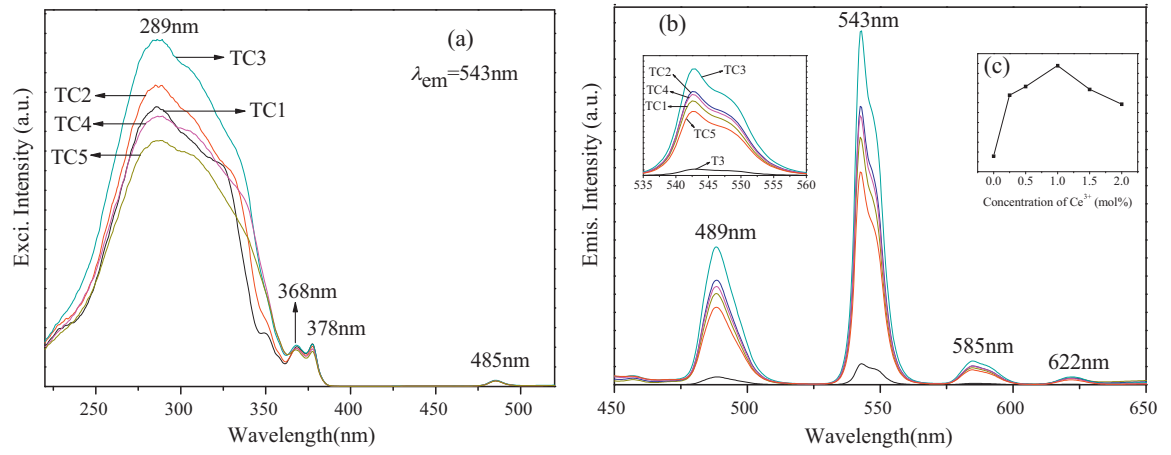

Fig. 6. Excitation (a) and emission (b) spectra of the Tb^{3+}/Ce^{3+} codoped glasses with different Ce-doping contents. (c) Emission intensities ($^5D_4 \rightarrow {}^7F_5$ transition of Tb^{3+}) as a function of Ce^{3+} concentration in the Tb^{3+}/Ce^{3+} codoped glasses. The emission spectrum and emission intensity of the (1.0 mol.%) Tb^{3+} ions doped glass are also presented in the figure for comparison.

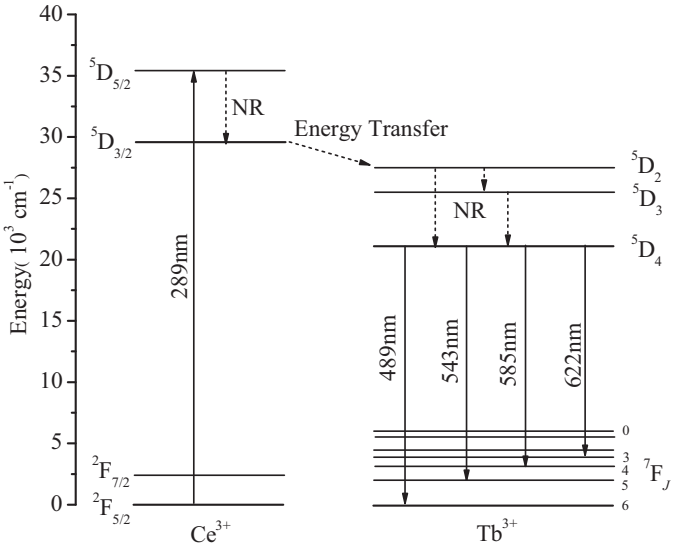

Fig. 7. Energy level scheme for energy transfer process from Ce^{3+} to Tb^{3+} ions in Tb^{3+}/Ce^{3+} codoped glasses.

returning from $^5D_{3/2}$ (Ce^{3+}) to the ground state is transferred to the UV absorption levels of Tb^{3+}, which decay non-radiatively to the excited level $^5D_4$ (Tb^{3+}) from which it decays radiatively down to the various underlying levels of ^5F_J (J = 6–3). As a result, the as-made Tb^{3+}/Ce^{3+} codoped glasses exhibit a strong green PL band centered at around 543 nm under 289 nm light excitation. It is well understood that increasing the concentration of Ce^{3+} ions would enhance the energy transfer rate from the $^5D_{3/2}$ level of Ce^{3+} to the $^5D_2$ level of Tb^{3+}, which would cause the high luminescence intensity of Tb^{3+} ions in the Tb^{3+}/Ce^{3+} codoped systems. Simultaneously, it is expected that the higher the Ce^{3+} concentration, the greater the fluorescence quenching because the probability of energy transfer to a second Ce^{3+} becomes higher. The most likely dominant mechanism for the concentration quenching of Ce^{3+} is energy migration to the neighboring Ce^{3+} ions in their ground state via cross-relaxation process [23]. The energy transfer probability that changes in proportion to the Ce concentration indicates that the Ce–Tb resonant energy transfer is mainly a dipole interaction.

4. Conclusions

In summary, Tb^{3+} or Ce^{3+} ions doped and Tb^{3+}/Ce^{3+} codoped oxyfluoride aluminosilicate glasses were successfully synthesized by the melt-quenching method. From XRD, DSC profiles the glass nature and their thermal properties have been understood. Transmission and excitation spectra have shown that all these glasses can be effectively excited by UV light. The Ce^{3+} excitation bands are due to the allowed transitions from the $^2F_{5/2}$ energy level to the splitting levels of 5d. The Tb^{3+} excitation bands are ascribed to absorption of the $4f^8 \rightarrow 4f^7 5d^1$ and $4f^8 \rightarrow 4f^8$ transitions of the Tb^{3+} ion. Upon UV excitation, the doped RE ions showed their characteristic emission, i.e., Ce^{3+} 5d–4f (blue) and Tb^{3+} $^5D_4 \rightarrow {}^7F_{J=6-3}$ (green) transitions. Concentration quenching is not observed even when Tb^{3+} is doped up to 8 mol.% in Tb^{3+} ions doped glass. This indicates that the as-made host glass can increase emission intensity and quenching concentration due to a good distribution of Tb^{3+} activators in glass matrix. PL excitation and emission spectra demonstrated that there is an efficient energy transfer from Ce^{3+} to Tb^{3+} through a non-radiative process in the codoped glasses, which resulted in enhanced green emission from them. Electric dipole–dipole interaction is mainly responsible for the energy transfer between Ce^{3+} and Tb^{3+} ions. Such efficient green light emission of the Tb^{3+}/Ce^{3+} codoped glasses makes them as excellent candidates for the opto-electronic materials and green colour display.

Acknowledgments

The authors acknowledge the financial support from the National Natural Science Foundation of China (No. 50672134) and the Science and Technology Bureau of Guangxi Province (Nos. 2010GXNSFB013018 and 2011GXNSFA018049).

References

[1] A. Agnesi, P. Dallocchio, F. Pirzio, G. Reali, Opt. Commun. 282 (2009) 2070.
[2] R.K. Verma, D.K. Rai, S.B. Rai, J. Alloys Compd. 509 (2011) 5591.
[3] J.E.C. Silva, G.F. de Sa, P.A. Santa-Cruz, J. Alloys Compd. 323–324 (2001) 336.
[4] K. Tonooka, N. Kamata, K. Yamada, F. Maruyama, J. Non-Cryst. Solids 150 (1992) 185.
[5] L. Zhu, C. Zuo, Z. Luo, A. Lu, Physica B 405 (2010) 4401.
[6] J. Ding, Q. Zhang, J. Cheng, X. Liu, G. Lin, J. Qiu, D. Chen, J. Alloys Compd. 495 (2010) 205.
[7] O.M. Ntwaeaborwa, H.C. Swart, R.E. Kroon, P.H. Holloway, J.R. Botha, J. Phys. Chem. Solids 67 (2006) 1749.
[8] S. Rai, S. Hazarika, Opt. Mater. 30 (2008) 1343.
[9] M. Nikl, J.A. Mares, E. Mihokova, K. Nitsch, N. Solovieva, V. Babin, A. Krasnikov, S. Zazubovich, M. Martini, A. Vedda, P. Fabeni, G.P. Pazzi, S. Baccaro, Radiat. Meas. 33 (2001) 593.
[10] Y. Chiu, W. Liu, Y. Yeh, S. Jang, T. Chen, J. Electrochem. Soc. 156 (2009) J221.
[11] D. Jia, J. Zhu, B. Wu, S.E. Paje, J. Lumin. 93 (2001) 107.
[12] L. Huang, X. Wang, H. Lin, X. Liu, J. Alloys Compd. 316 (2001) 256.
[13] T. Tsuboi, Eur. Phys. J. Appl. Phys. 26 (2004) 95.
[14] D. He, C. Yu, J. Cheng, S. Li, L. Hu, J. Alloys Compd. 509 (2011) 1906.
[15] Q. Luo, X. Qiao, X. Fan, X. Zhang, J. Non-Cryst. Solids 356 (2010) 2875.
[16] C. Zuo, A. Lu, L. Zhu, Mater. Sci. Eng. B 175 (2010) 229.
[17] J. Fu, J.M. Parker, R.M. Brown, P.S. Flower, J. Non-Cryst. Solids 326–327 (2003) 335.
[18] Y.P. Naik, M. Mohapatra, N.D. Dahale, T.K. Seshagiri, V. Natarajan, S.V. Godbole, J. Lumin. 129 (2009) 1225.
[19] B.V. Rao, Y.T. Nien, W.S. Hwang, I.G. Chen, J. Electrochem. Soc. 156 (2009) 338.
[20] G. Lakshminarayana, R. Yang, J. Qiu, M.G. Brik, G.A. Kumar, I.V. Kityk, J. Phys. D: Appl. Phys. 42 (2009) 015414.
[21] Z. Xu, Y. Li, Z. Liu, D. Wang, J. Alloys Compd. 391 (2005) 202.
[22] A. Thulasiramudu, S. Buddhudu, Spectrochim. Acta A 66 (2007) 323.
[23] L. Zhu, X. Wang, G. Yu, X. Hou, G. Zhang, J. Sun, X. Liu, D. Xu, Mater. Res. Bull. 43 (2008) 1032.